

Article

Robust Control of Small Turbojet Engines

Rudolf Andoga ^{1,*}, Ladislav Főző ¹, Radovan Kovács ¹, Károly Beneda ², Tomáš Moravec ¹ and Michal Schreiner ¹

¹ Technical University of Košice, Faculty of Aeronautics, Rampová 7, 041 21 Košice, Slovakia; ladislav.fozo@tuke.sk (L.F.); radovan.kovacs@tuke.sk (R.K.); tomas.moravec@tuke.sk (T.M.); michal.schreiner@tuke.sk (M.S.)

² Department of Aeronautics, Naval Architecture and Railway Vehicles, Faculty of Transport Engineering, Budapest University of Technology and Economics, H-1521 Budapest, P.O.B. 91, Hungary; kbeneda@vrht.bme.hu

* Correspondence: rudolf.andoga@tuke.sk; Tel.: +421 55 602 6140

Received: 2 October 2018; Accepted: 17 December 2018; Published: 4 January 2019



Abstract: Modern turbojet engines mainly use computerized digital engine control systems. This opens the way for application of advanced algorithms aimed at increasing their operational efficiency and safety. The theory of robust control is a set of methods known for good results in complex control tasks, making them ideal candidates for application in the current turbojet engine control units. Different methodologies in the design of robust controllers, utilizing a small turbojet engine with variable exhaust nozzle designated as iSTC-21v, were therefore investigated in the article. The resulting controllers were evaluated for efficiency in laboratory conditions. The aim was to find a suitable approach and design method for robust controllers, taking into account the limitations and specifics of a real turbojet engine and its hardware, contrary to most studies which have used only simulated environments. The article shows the most effective approach in the design of robust controllers and the resulting speed controllers for a class of small turbojet engines, which can be applied in a discrete digital control environment.

Keywords: turbojet engine; robust control; iSTC-21v; discrete control; advanced control

1. Introduction

Design of control systems for a turbine engine requires knowledge from many science fields, including aerodynamics, fluid mechanics, thermodynamics, rigid body mechanics, chemistry, and material sciences [1]. Each designed control system has to keep the controlled engine within certain operational limits, as depicted in Figure 1. These limits are defined by the maximal rotational speed and exhaust gas temperature, as well as by the surge line represented by the coefficient of excess air in the main combustion chamber. This means that the control system has to operate in a complex environment and respect the constraints of a multi-dimensional non-linear space with many uncertainties [1].

In order to solve the aforementioned problems and deal with uncertainties in the control of turbojet engines, the methodology of robust control, as described in fundamental literature [2–5], can be applied. The reported results show that this methodology can achieve a high quality of control in a broad spectrum of operational states of complex systems. Therefore, it can be deemed a suitable candidate for application in the efficient control of turbojet engines [6]. Based on current research in robust control of turbojet engines, the method mainly applied in turbine engine control in current publications is the \mathcal{H}_∞ norm-based control [7,8].

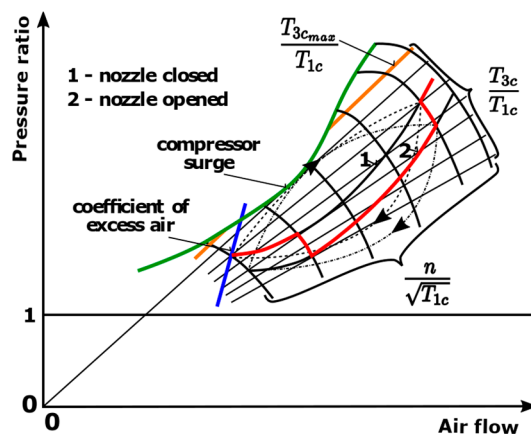


Figure 1. Turbine engine with variable exhaust nozzle compressor characteristics with control borders.

However, application of the methodology is often done in virtual environments only [8,9]. The aim of the present paper is to show and demonstrate the application of this methodology in an environment with physical systems, taking into account all limitations and specifics, such as discrete forms of robust controllers, data delays, and limited action hits, all within a variable operational envelope. In a simulated environment, using \mathcal{H}_∞ norm-based controllers as part of a turbine engine control system and the impact of those controllers on the engine's control system stability and performance have already been studied [7]. The aim of the study was to design a robust controller with the smallest possible output and power consumption [7]. It was also proved that robust controllers are generally better in performance and stability than the classical control approach using proportional-integral-derivative (PID) controllers using a simulated turbojet engine [8]. Operation in real world conditions is, however, different from such ideal calculations in a simulated continuous state space, as the measured data are often delayed and the controller operates in a discrete state space. Such uncertainties, represented by data delays or drop-outs, were modeled in a distributed aero engine control system [9]. The paper describes an \mathcal{H}_∞ controller designed to control the whole engine's operating envelope, but again, the results were only obtained in a simulated environment.

The possibilities of application of robust control in turbine engines in advanced intelligent frameworks were also studied [1]. Nonlinear behavior and uncertainty of a turbine engine with deterioration was taken and compensated by its robust control system. Using simulations with the C-MAPSS40k model, it was proven that robust controllers can effectively control a turbine engine with the mentioned types of modeled uncertainties [10]. Data delays or dropouts in a distributed control system with impacts on uncertainty modeling as well as stability and performance of the robust control system of a turbine engine were also studied in simulated environment [11]. Compared to predictive or classic PID controllers, robust controllers have achieved higher control quality in speed and temperature control of a gas turbine power plant [12]. In the same study, robust controllers were tested together with the nonlinear autoregressive model, using exogenous inputs (NARX). All robust controllers were designed using the experimental NARX models and were designed using the \mathcal{H}_∞ method. In addition, researchers from NASA Glen Centre [13] used robust control to preserve control system properties even during engine degradation, either over time or for other reasons. They used the Lyapunov parametric depending function to design a parameter dependent control system. The robust control system was able to adapt using performance weights depending on coefficients, which were determined by the index of the engine's degradation. Robust tracking control of turbofan engines using the \mathcal{H}_∞ Leitmann method was applied with good results in attenuation of the engine's uncertainties [14]. By numerical simulations, the authors in the paper proved very good performance in stability of a turbofan engine tracking control.

The robust control approach has also successfully been applied in other engineering and aviation topics in technical practice. The classical root locus and \mathcal{H}_∞ methods were investigated in the design

of the well-known C* flight control algorithm, in order to compare advantages and disadvantages of both approaches [15]. The root locus approach was faster and simpler to apply but gave conservative results, while the advanced \mathcal{H}_∞ controller was better in uncertainty attenuation but more difficult to design [15]. In another aviation application, the \mathcal{H}_∞ theory was successfully used to fight the nonlinear behavior of autonomous aerial vehicles [16]. A nonlinear, predictive robust controller was better in control of an autonomous plane, even with data delays, plane degradation, and instability, compared to linear controllers. The problem of vessel positioning control was also solved using \mathcal{H}_∞ and μ synthesis, with good simulation results in frequency and time domain [17]. An efficient combination of fuzzy control and robust control strategies were applied to design the controllers for solar collector fields [18]. An efficient control framework for discrete nonlinear systems using a state dependent Riccati equation solution was also successfully developed using the methodology of robust control, showing very promising results on an inverted pendulum [19].

The motivation behind the present research was to apply working approaches in robust controller design, and test them in control of a small turbojet engine in order to determine the resulting control efficiency. The aim, and the expected scientific contribution, was to research and identify the methods and approaches that will be suitable and applicable in developing digital control systems for this class of turbojet engines. This research should also answer the question of whether the design of robust controllers, which is a quite complex task, can feasibly be applied in the real-time environment of a digital control system of turbojet engines, compared to traditional control design approaches. Contrary to most simulation studies presented in the introduction, the result of this study is intended to be a pioneering practical application of robust control in a digital control system of a small turbojet engine, and it may support further developments in the control of such engines in aviation applications.

2. Modeling the iSTC-21v Engine with Uncertainties

In order to design a robust control system, a model of the engine and its uncertainties must be designed. An experimental identification approach was selected to design a set of dynamic models, suitable for design of robust controllers. As a data source, a small turbojet engine iSTC-21 was employed, as shown in Figure 2. The engine was operated in laboratory conditions with a digital data acquisition system measuring the most important input, output, state, and environmental variables, with a sampling rate set as $f_s = 10$ Hz. The data acquisition system, measured parameters, and the resulting data are described in detail in References [20–22]. In the specific case of robust controller design, the nonlinearity of a turbine engine can be taken as its uncertainty. Therefore, it was necessary to design a set of linearized models of different operating points of the engine, which covered its whole operational envelope. The transfer function defining the structure of the individual linear models is defined by Equation (1). This model structure was selected according to the previous experiments described in References [21–23]. The resulting model after Laplace transformation, which is valid for the i -th operational point, described the dynamic dependence of the engine's speed $n(s)$ on the control variable of fuel flow - $FF(s)$ (Equation (1)). The aim of the identification process was to find the coefficients a_i and b_j .

$$F_i(s) = \frac{a_1s + a_0}{b_2s^2 + b_1s + b_0} = \frac{n(s)}{FF(s)} \quad (1)$$

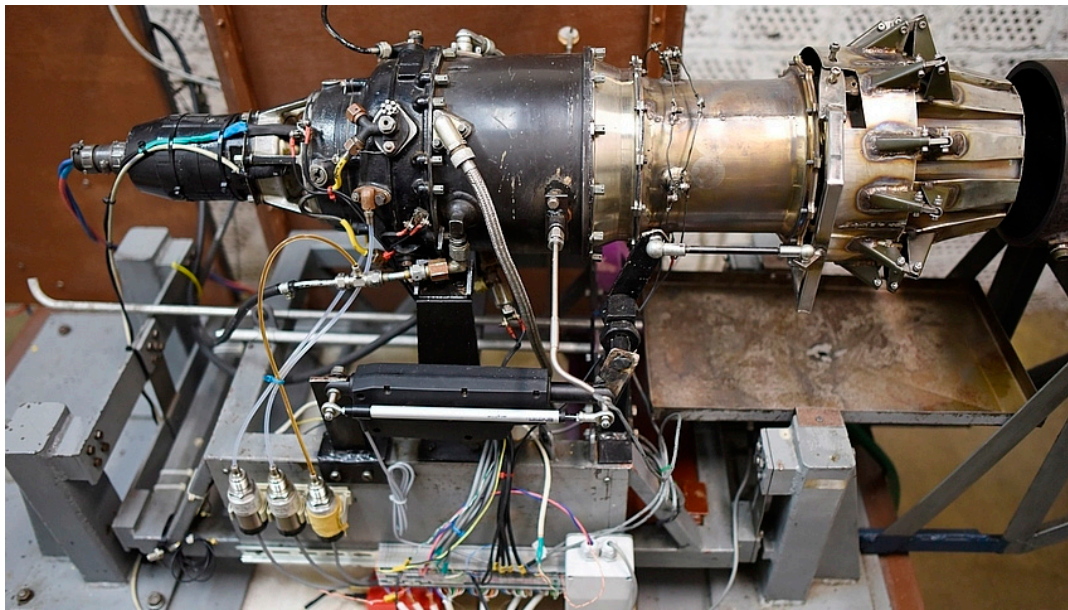


Figure 2. An iSTC-21v small turbojet engine on a test bench.

Figure 3 shows the measured dynamic engine data used for identification of linearized models for the six operational points defined as OP1 ... OP6, while the resulting transfer functions were designated as $F_1(s) \dots F_6(s)$.

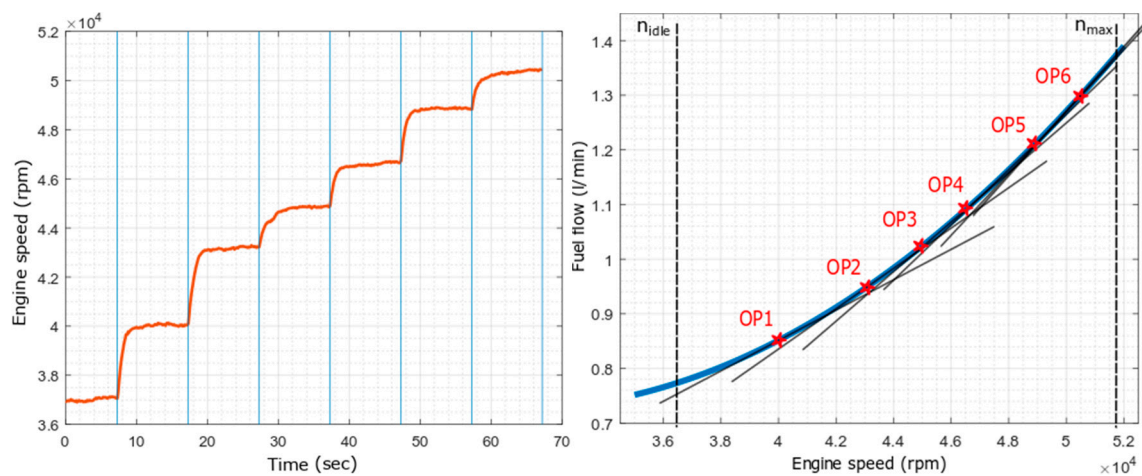


Figure 3. The measured dynamic input data used for identification and modeling.

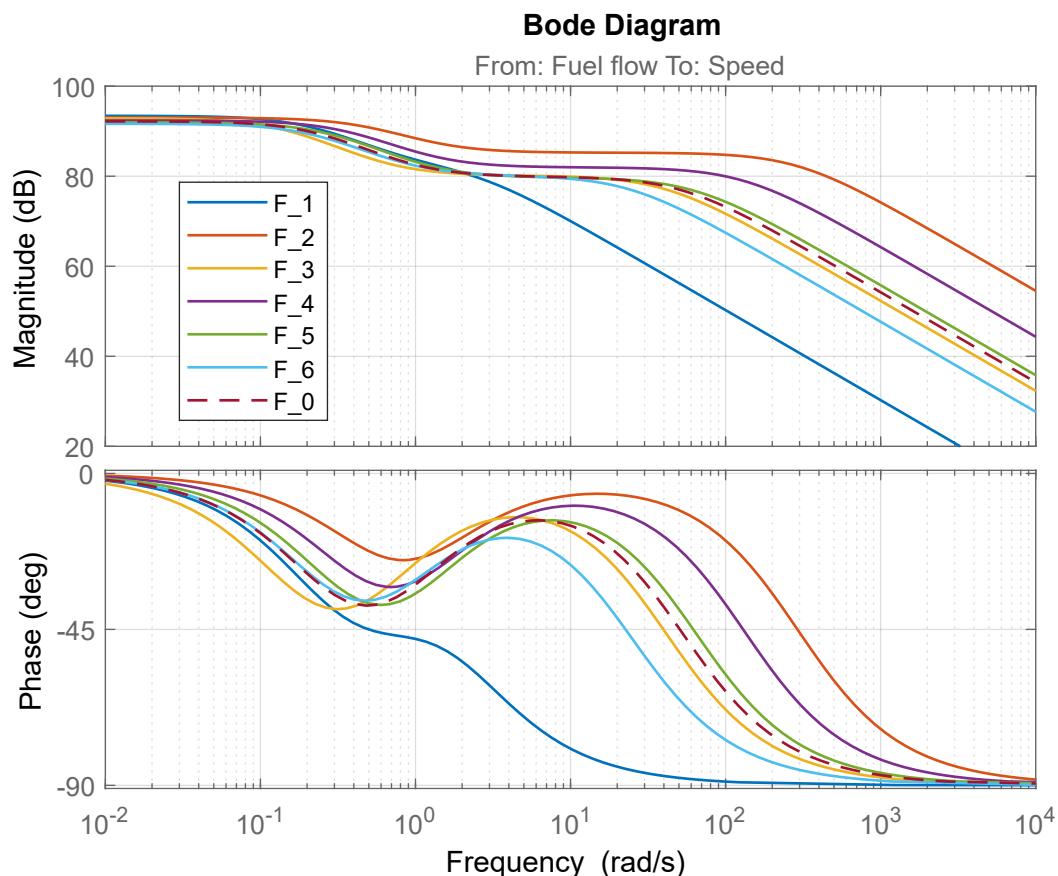
A model for each operational point was constructed; the obtained models, using an experimental identification methodology [21,22], are summarized and given in Table 1. The models were evaluated using standard metrics, the mean absolute error (MAE), and the maximum absolute error (MAAE), as well as their percentage expressions (MAAPE and MAPE). The table shows that, using the methodologies presented in the previous publications [21–24], it was possible to achieve a precision with average errors lower than 1%. These models were used to determine the uncertainties applied in the design of robust controllers. The frequency response of the individual models is shown in Figure 4. It can be seen that the models had a high gain, they were thus highly susceptible to changes in control inputs and noise.

Table 1. Dynamic linearized models of the engine in different operational points.

Operational Point (OP)	MAE (rpm)	MAPE (%)	MAAE (rpm)	MAAPE (%)	Individual Transfer Functions $F_i(s)$
1.	37.3312	0.2714	109.9996	0.0931	$F_1(s) = \frac{6449s + 2.82 \times 10^4}{s^2 + 2.156s + 3.389}$
2.	76.3130	0.1778	621.0031	1.4112	$F_2(s) = \frac{8219s + 1.338 \times 10^4}{s^2 + 3.298s + 1.936}$
3.	35.1434	0.0778	132.2502	0.2889	$F_3(s) = \frac{2828s + 1020}{s^2 + 1.121s + 0.1625}$
4.	34.1676	0.0721	175.5602	0.3669	$F_4(s) = \frac{4758s + 3.959 \times 10^4}{s^2 + 4.619s + 7.126}$
5.	37.7333	0.0762	110.1576	0.2215	$F_5(s) = \frac{1154s + 2758}{s^2 + 2.31s + 0.5891}$
6.	30.8231	0.0607	187.9138	0.3676	$F_6(s) = \frac{5865s + 3126}{s^2 + 3.326s + 0.7489}$

The nominal engine model was computed as a mean of the individual model's coefficients ($F_1(s) \dots F_6(s)$), with the resulting transfer function defined as follows in Equation (2) [2,3,25]:

$$F_0(s) = \frac{4879s + 1.468 \times 10^4}{s^2 + 2.805s + 2.325} \quad (2)$$

**Figure 4.** Frequency characteristics of the individual linearized engine models $F_0(s) \dots F_6(s)$.

As an example of the obtained precision as demonstrated in Table 1, the linear model for the operating point OP1 was selected and the results shown in Figure 5. In the left part of Figure 5, the measured fuel flow is shown (note small oscillations in fuel flow supply). The middle part shows the dynamic response of the model with the engine accelerating to a speed of 40,500 rpm, defining the operational point 1. The right part of the figure shows the model as the amplitude frequency characteristics.

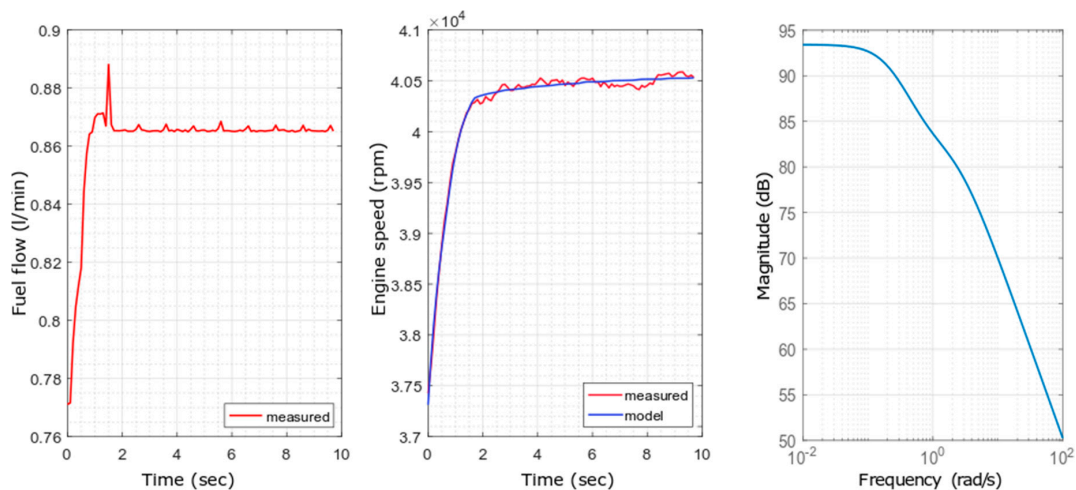


Figure 5. Dynamic simulation of the model for the first operating point OP1.

As the resulting model for a robust controller design, the nominal engine model $F_0(s)$ was used. On top of the model, Equation (3), showing the additive dynamic uncertainty, and Equation (4), presenting the multiplicative dynamic uncertainty were used in our investigation into the design of robust controllers [2–4].

$$F(s) = F_0(s) + w_a(s) \cdot \delta(s) \quad (3)$$

$$F(s) = F_0(s) \cdot [1 + w_m(s) \cdot \delta(s)] \quad (4)$$

where

- $F_0(s)$ represents the nominal model of the dynamic system, in this case a small turbojet engine described in Equation (2).
- $w_a(s)$ represents the transfer function of the additive uncertainty.
- $w_m(s)$ represents the transfer function of the multiplicative form of uncertainty.
- $\delta(s)$ represents the absolute value of the uncertainty in the interval: $\langle -1, 1 \rangle$.

For the small turbojet engine iSTC-21v, the following transfer functions of the uncertainties, using the models $F_1(s) \dots F_6(s)$, were obtained:

$$w_a(s) = \frac{0.00159s^2 + 5751s + 7632}{s^2 + 1.309s + 1.998} \quad (5)$$

$$w_m(s) = \frac{0.7856s^2 + 4.171s + 1.593}{s^2 + 3.073s + 3.114} \quad (6)$$

Having computed the nominal model of the engine $F_0(s)$, and computed its uncertainties using linearized models across six operational points, the robust controllers could be designed. After preliminary tests and initial design of controllers, the additive uncertainty as modeled in Equation (5) was selected and applied in the following sections.

3. Robust Control Design

Two different approaches in the design of controllers were applied, based on well-known robust control theories. The aim was to evaluate the efficiency of small gain theory and the methods based on the \mathcal{H}_∞ norm [2–4]. The aim was to find the most efficient approach suitable for a small turbojet engine, as well as to define a robust speed controller that can be applied for this class of engines. Comparison of results between simulated (synthetic) environments and tests in laboratory conditions with a real engine can also provide valuable knowledge, which can be applied in the follow-up design of robust

speed controllers. Because the simulation models of the engine were designed in continuous time, methodologies in continuous time [3–5] were applied in design of the controllers, and the calculated controllers were afterwards discretized for implementation in a digital control system.

3.1. The Small Gain Theory

For robust controllers written in the classical proportional-integral-derivative (PID) form, a method developed by Vesely and Harsanyi was used [5]. The method is based on small gain theory, and a full description can be found in the mentioned publication. The small gain theory was chosen because of its fundamental place in robust control theory and proven results in control of complex systems [2–4]. Two approaches for design of PID controllers using the small gain theory were developed [5]. The first one is based on direct controller synthesis, with respect of the object’s uncertainty. The module of the design function must be below the maximal module of the controlled object’s uncertainty [5].

$$|T_0(\omega)| < \frac{F_0(j\omega)}{w(j\omega)} = M_0(\omega) \tag{7}$$

where $w(j\omega)$ is the system’s uncertainty module and $M_0(\omega)$ is the maximal module of the uncertain closed loop control system. The coefficients of the controller can then be calculated as follows, using the chosen closed loop transfer function $W(j\omega)$ [5]:

$$W(j\omega) = |T_0(\omega)| = \frac{R(j\omega)F_0(j\omega)}{1 + R(j\omega)F_0(j\omega)} \tag{8}$$

where $R(j\omega)$ is the resulting controller transfer function achieved by derivation of Equation (7). The conditions that must be satisfied are presented in Figure 6.

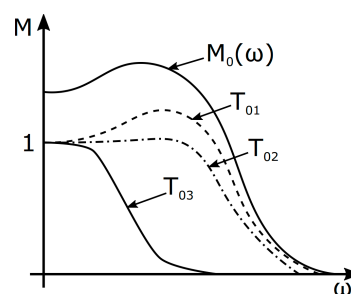


Figure 6. Closed loop control module $T_0(\omega)$ and the uncertainty module $M_0(\omega)$.

The comparison of the designed controller in a closed feedback loop scheme, marked as CL, is shown in Figure 7. All curves of the uncertain model are close to the design curve $W(j\omega)$, and it lies below the max of the uncertainty module $M_0(j\omega)$.

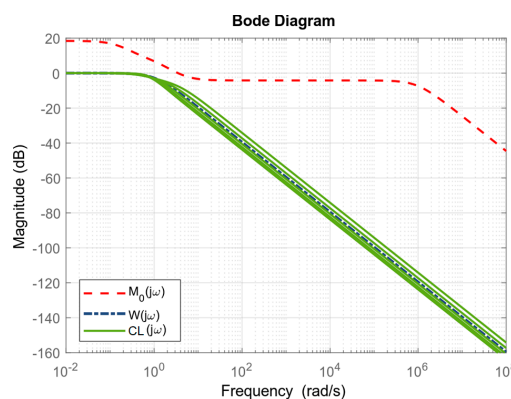


Figure 7. Bode diagram of designed PID controller in a closed loop (CL), and design restrictions W and M_0 .

The second method is based on a nominal model denominator comparison, and once again the closed loop module should be under the controlled object's uncertainty [5]. By applying this algorithm, the resulting equation for the PID controller is shown below [5]:

$$a_3s^3 + a_2s^2 + a_1s + a_0 = (d_1s + 1)(c_1s^2 + c_0s + c_{-1}) \quad (9)$$

On the left side of the equation is the system's transfer function denominator, and on the right side is the complementary polynomial $D(s)$, and the controller's coefficients without any gain. The gain is a chosen value, and the only limitation is that the closed loop transfer function must lie below the maximal uncertainty module $M_0(\omega)$. The resulting coefficients of the PID controller can be expressed as follows [5]:

$$F_c(s) = \frac{r_1s^2 + r_0s + r_{-1}}{s} = \frac{\frac{c_1}{K}s^2 + \frac{c_0}{K}s + \frac{c_{-1}}{K}}{s} \Rightarrow P = \frac{c_0}{K}, I = \frac{c_{-1}}{K}, D = \frac{c_1}{K} \quad (10)$$

3.2. H-Infinity Control

Two methods using the \mathcal{H}_∞ norm of the closed loop system were selected to design robust controllers: the loop shaping method and the mixed sensitivity method. The \mathcal{H}_∞ optimization was selected because of its high quality, efficient robust design, and also good simulation results from in the state of the art analyses published by previous authors.

3.2.1. Loop Shaping

The Glover McFarlane algorithm was used as a loop shaping method, based on normalized coprime factorization of the controlled system [2,26]. The first step was to select pre- and post-compensators W_1 and W_2 so that the gain of the shaped plant $F_s = W_2GW_1$ was low at frequencies where good disturbance attenuation was required, and was sufficiently high at frequencies where good robust stability was required. The second step was to use the *ncfsyn* Matlab function to compute the optimal positive feedback controller R [2].

The resulting controller was defined as follows (11):

$$R = W_2R_\infty W_1 \quad (11)$$

and it simultaneously minimized two \mathcal{H}_∞ cost functions (12,13):

$$\gamma := \min_R \left\| \begin{bmatrix} I \\ R \end{bmatrix} (I - F_s R)^{-1} [F_s, I] \right\|_\infty \quad (12)$$

$$\gamma := \min_R \left\| \begin{bmatrix} I \\ F_s \end{bmatrix} (I - R F_s)^{-1} [R, I] \right\|_\infty \quad (13)$$

A more detailed description of the applied algorithm can be found in References [2,26].

The second loop shaping method used the *loopsyn* Matlab function. Based on the desired loop shape as defined by the transfer function F_d , it computed a stabilizing \mathcal{H}_∞ controller to shape the Df singular value of the loop transfer function FK , resulting in the desired loop shape with the desired accuracy γ , in the sense that if $\omega_0 = 0$ db at the crossover frequency of the singular value of the transfer function $F_d(j\omega)$, then [1]:

$$\underline{\sigma}(F(j\omega)R(j\omega)) \geq \frac{1}{\gamma} \underline{\sigma}(F_d(j\omega)) \text{ for all } \omega > \omega_0 \quad (14)$$

$$\underline{\sigma}(F(j\omega)R(j\omega)) \leq \gamma \underline{\sigma}(F_d(j\omega)) \text{ for all } \omega > \omega_0 \quad (15)$$

Full description of the applied algorithm for computation of Equations (14) and (15) can be found in Reference [2].

3.2.2. Mixed Sensitivity

The second applied method was synthesis using mixed sensitivity. The **mixsyn** Matlab function computes a controller R that minimizes the \mathcal{H}_∞ norm of the closed loop transfer function using the mixed sensitivity [1].

$$\left\| \begin{bmatrix} W_1 S \\ W_2 K \\ W_3 T \end{bmatrix} \right\|_\infty \quad (16)$$

The resulting controller R is such that S , K and T satisfy the following loop shaping inequalities:

$$\bar{\sigma}(S(j\omega)) \leq \gamma \underline{\sigma}(W_1^{-1}(j\omega)) \quad (17)$$

$$\bar{\sigma}(K(j\omega)) \leq \gamma \underline{\sigma}(W_2^{-1}(j\omega)) \quad (18)$$

$$\bar{\sigma}(T(j\omega)) \leq \gamma \underline{\sigma}(W_3^{-1}(j\omega)) \quad (19)$$

where γ is accuracy. The inverses of the W_1 and W_3 weights determine the shapes of the sensitivity function S and the complementary sensitivity function T . Typically, a large W_1 is chosen inside the desired control bandwidth, to achieve good disturbance attenuation (performance). A large W_3 value is typically chosen outside the control bandwidth for good stability (robustness) [2,26].

4. Simulation and Experimental Results

Simulations and implementation of the calculated controllers were realized using a closed loop feedback speed control scheme, as shown below in Figure 8. The controllers were discretized using a sampling period set as $T_s = 0.01$ sec.

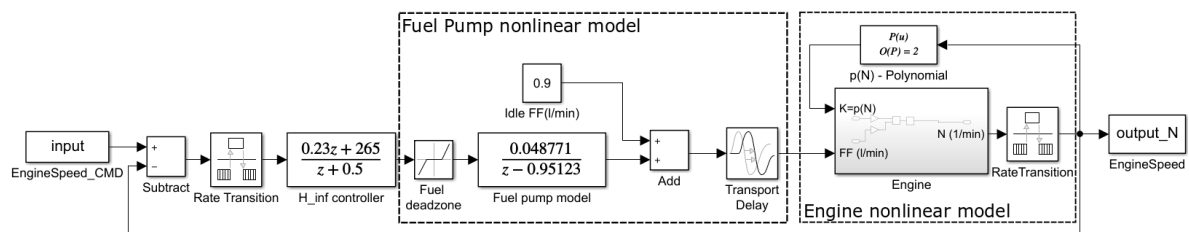


Figure 8. Simulation and implementation scheme.

Evaluation of the calculated robust controllers in simulation environment was realized using a nonlinear model of the iSTC-21v [21,22]. This model is able to describe both the multi-mode operating envelope and some delays, which are caused by the engine's systems as well its own dynamics. In laboratory conditions these are the most significant uncertainties, because all other ambient/environmental conditions are relatively stable. The simulation results show that the H-infinity controller designed using the loop shaping methodology approach accelerated the engine through step changes in the operational speed set-points, up to its theoretical maximum speed limit. These simulation results showed that the controller was stable and could be tested on a real small turbojet engine on a test bench. The best performing robust controllers were the small gain robust controller (SG) and the \mathcal{H}_∞ robust controller. These two controllers were compared to a classical PI controller designed using the optimal module methodology [20]. The experiment in a simulated environment, as presented in Figure 9, showed that all three controllers were very smooth in operation and were able to control the engine with sufficient control quality. The next step was to use the

best performing controllers and test them on a real object—the small turbojet engine iSTC-21v—by updating its control system.

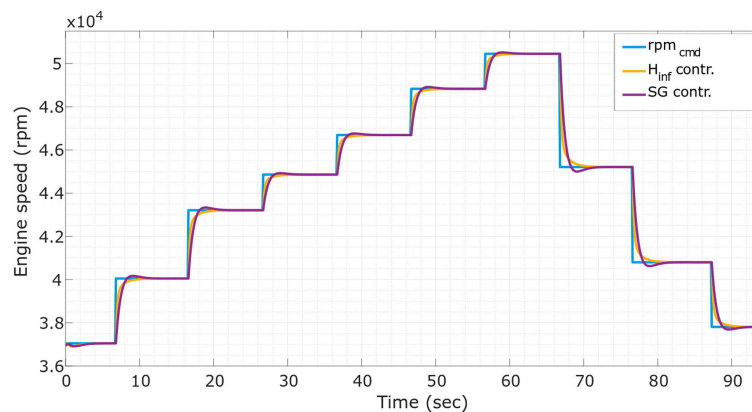


Figure 9. Simulation results on the chosen operating points of the iSTC-21v engine.

Figure 10 illustrates the response of the individual controllers in a laboratory test, using the iSTC-21v engine running on a test bench with a real-time data acquisition control system, with the tested controller implemented in a situational control system [20] without switching, and using only a single controller throughout the whole operating range of the engine. The first set of test results, presented in Figure 9, shows the controllers responding to a step change in the set-point control signal, accelerating the engine from the operating point of $N_{idle} = 40,000$ rpm to the operating point defined by the command signal $N_{command} = 46,000$ rpm. The command signal is shown as a blue line in Figure 9, and the responses of the individual controllers designed by the small gain method, the \mathcal{H}_∞ method, and an optimal PI controller are also shown. All controllers performed in an acceptable manner, robust controllers having faster acceleration at the physical limits of the fuel pump and the engine itself.

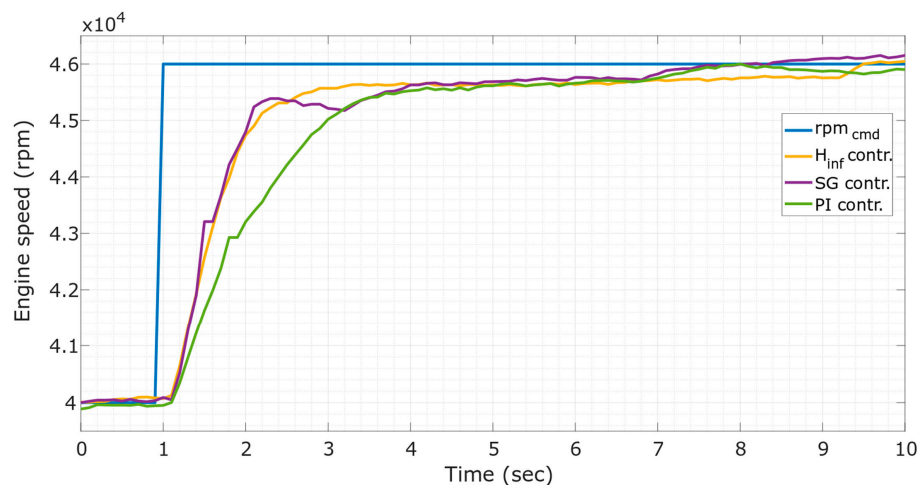


Figure 10. Engine speed controlled by robust controllers and a PI controller—single step response.

The other test, which illustrated the performance of the designed controllers showed step accelerations of the engine nearly up to the maximal speed of the engine $N_{command} = 49,000$ rpm. As can be seen in the results, all controllers exhibited slightly oscillatory behavior around certain operational points, namely the idle operational point, defined at $N_{command} = 38,000$ rpm, and the operational point $N_{command} = 43,000$ rpm.

The oscillations are believed to have been caused by high susceptibility of the controlled system to very small changes in fuel flow supply from the fuel pump, as shown in the Bode diagrams in Section 2. They could also be attributed to the age of the engine and ageing effects on its fuel system and nozzle

construction. To get rid of these effects in the iSTC-21v engine, it would be necessary to replace the fuel nozzles and improve the fuel supply system. These oscillations could be attenuated by the controllers by increasing the response times of the controller, however, this would go against the design aim to have the engine accelerated as fast as possible. Another solution to this problem would be the application of a situational control system with switched controllers, where this oscillatory behavior was eliminated using specifically designed controllers for stable conditions with higher robustness, albeit slower response [20]. The obtained controllers are given in a discrete form in Table 2.

Table 2. The resulting robust controllers in a discrete form for application in digital control systems.

Controller	Discrete Transfer Function Controllers—Sample Time: 0.01 s
SG	$F_{SG}(z) = \frac{5.932 \times 10^{-5} z^2 + 6.584 \times 10^{-7} z - 5.866 \times 10^{-5}}{z^2 - 0.09298z - 0.907}$
\mathcal{H}_∞	$F_{\mathcal{H}_\infty}(s) = \frac{3.363 \times 10^{-5} z^3 + 3.087 \times 10^{-5} z^2 - 3.292 \times 10^{-5} z - 3.016 \times 10^{-5}}{z^3 + 0.8139z^2 - 0.9913z - 0.8225}$
PI	$F_{PI}(z) = \frac{2.429 \times 10^{-5} z - 2.4 \times 10^{-5}}{z - 1}$

The experiments showed that robust controllers have a slight advantage over the classical optimal PI controller in performance. The performance of the individual controllers is shown in Table 3. Acceleration characteristics were defined according to the criteria of settling time, defining the time it took for the speed to reach 90% of the commanded speed, and maximal overshoot of the controller averaged across six operational points as shown in Figure 11. In the steady state where the speed was stable, mean average error across six operational points, shown in Figure 11, was evaluated. We can see that the lowest settling time and the best transitional behavior (during acceleration) is obtained by using the \mathcal{H}_∞ controller. In steady state the robust \mathcal{H}_∞ was slightly better in mean absolute error than the small gain robust controller. The PI controller designed by the optimal module design method had the worst performance, although it was still acceptable for application in a small turbojet engine.

Table 3. Statistical evaluation of the designed controllers.

Controller	Transition State		Steady State			
	Settling Time (sec)	Max. Overshoot (%)	MAE (RPM)	MAPE (%)	MAAE (RPM)	MAAPE (%)
SG	5.115	0.435	111.805	0.245	284.405	0.615
\mathcal{H}_∞	2.7833	0.788	101.532	0.2347	285.4147	0.6507
PI	3.244	0.8215	157.3056	0.3594	396.0219	0.89

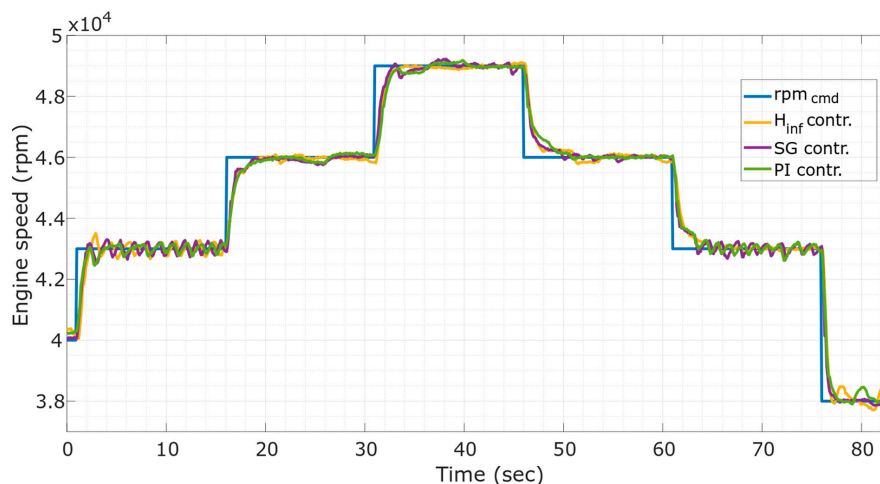


Figure 11. Engine speed controlled by robust controllers and a PI controller—multi step response.

5. Conclusions and Discussion

The results, obtained in simulation and laboratory experiments, show that a robust control approach can be applied to control the speed of a small iSTC-21v turbojet engine. This means that the theory of robust control can be successfully applied to a real turbojet engine using a digital control system. A suitable approach to design of robust controllers has been found, which can be further built on and applied in this class of small turbojet engines. The recommended dynamic model for use in design of robust controllers for small turbojet engines is a second order nominal model, computed as an average across several operational points covering the operational envelope and expanded by additive uncertainties.

The dynamic engine models presented in the paper are suitable for design of robust controllers for small turbojet engines with static thrust from 50 up to 100 kilograms. The developed nominal model can be used in design of a robust controller; the best performing method in laboratory conditions and using a digital control system was the H-infinity method, using the loop shaping approach in its design as described in section three. The robust controllers, which are deemed to be suitable for the class of small turbojet engines, are given in Table 2. It needs to be noted here that all designed robust controllers performed flawlessly in simulated environment, however when implemented on a real engine in laboratory experiments that was not always case, as the controllers oscillated at certain operational points. This illustrates the fact that good simulated performance of a robust controller does not guarantee similar performance in a physical system. Transition times during acceleration were improved by about 0.5 seconds using robust controllers, the maximal overshoot was decreased, and other comparative criteria were also improved as shown in Table 3.

In conclusion, it can be said that the improvement using robust controllers on a real turbojet engine is rather marginal when dealing with an engine at the ground level. Higher uncertainty would be present when using the engine in flight conditions, where the outer environment has a significant impact on its thermodynamic performance. It can be hypothesized that robust controllers would significantly improve performance of the engine in these conditions, however, the designed uncertainties would have to be recalculated. Performance could be further enhanced by application of algorithms from the area of computational intelligence, as illustrated in some recent works [27,28]. Another path would be to test the possible application of additive and multiplicative uncertainties to improve results [29]. More complex tests resembling certain flight conditions can be done using the variable exhaust nozzle of the iSTC-21v engine in future experiments.

Author Contributions: Conceptualization, R.A. and L.F.; Data curation, R.A., L.F. and R.K.; Formal analysis, R.A., L.F. and R.K.; Investigation, R.A., L.F., R.K., T.M. and M.S.; Methodology, R.A., L.F., R.K. and K.B.; Software, L.F. and R.K.; Supervision, R.A., L.F. and K.B.; Validation, L.F., R.K., K.B., T.M. and M.S.; Visualization, L.F., R.K., T.M. and M.S.; Writing—original draft, R.A., L.F. and R.K.; Writing—review & editing, R.A. and L.F.

Funding: The work was supported by projects: ESPOSA—‘Efficient Systems and Propulsion For Small Aircraft’, funded by the European commission in the seventh frame work program under the grant agreement no. ACP1-GA-2011-284859-ESPOSA, and APVV—Slovak Research and Development Agency under grant agreement no. DO7RP-0023-11.

Conflicts of Interest: The authors declare no conflict of interest.

Nomenclature

ARX	Auto regressive Model with Exogenous Input
C*	The C Star Algorithm for Aircraft Attitude Control
EGT	Exhaust Gas Temperature
FADEC	Full Authority Digital Engine Control
FF	Fuel Flow
H-inf	H Infinity Method
iSTC-21v	Intelligent Small Turbo-Compressor Engine -21 with Variable Exhaust Nozzle
MAE	Mean Absolute Error
MAPE	Mean Absolute Percentage Error

MAAE	Maximum Absolute Error
MAAPE	Maximum Absolute Percentage Error
n	The Speed of the Engine
NARX	Non Linear Autoregressive Model with Exogenous Input
OP	Operational Point
PID	Proportional Integral Derivative Controller
RPM	Revolutions per Minute
SG	Small Gain Controller
T _{1C}	Temperature on the Compressor Inlet
T _{3C}	Temperature on the Compressor Outlet

References

- Jaw, L.; Mattingly, J. *Aircraft Engine Controls: Design, System Analysis, and Health Monitoring*; AIAA Education Series; American Institute of Aeronautics and Astronautics: Reston, VA, USA, 2009; ISBN 978-1-60086-705-7.
- Gu, D.W.; Petkov, P.; Konstantinov, M.M. *Robust Control Design with MATLAB®*; Advanced Textbooks in Control and Signal Processing; Springer: London, UK, 2014; ISBN 978-1-4471-4682-7.
- Zhou, K.; Doyle, J. *Essentials of Robust Control*; Prentice Hall Modular Series; Prentice Hall: Upper Saddle River, NJ, USA, 1998; ISBN 978-0-13-525833-0.
- Green, M.; Limebeer, D. *Linear Robust Control*; Dover Books on Electrical Engineering; Dover Publications: Mineola, NY, USA, 2013; ISBN 978-0-486-26509-4.
- Vesely, V.; Harsanyi, L. *Robust Control: Applications (Robustné Riadenie: Aplikácie)*; Slovak Technical University in Bratislava STU: Bratislava, Slovak, 2015; ISBN 978-80-227-4339-6.
- Főző, L.; Andoga, R.; Madarász, L.; Kolesár, J.; Judičák, J. Description of an intelligent small turbo-compressor engine with variable exhaust nozzle, in with variable exhaust nozzle. In Proceedings of the IEEE 13th International Symposium on Applied Machine Intelligence and Informatics (SAMII), Herľany, Slovakia, 22–24 January 2015; pp. 22–24.
- Alikhani, H.R.; Motlagh, M.M. Aero Engine Multivariable Robust Control. *Tech. J. Eng. Appl. Sci.* **2016**, *5*, 228–232.
- Baniassadi, A.; Markazi, A.H.D.; Karami, M. Robust control of a gas turbine with wiener model uncertainty. *Indian J. Sci. Technol.* **2012**, *5*, 3584–3592.
- Peng, J.; Zhang, Z.; Feng, F. H_∞ Optimal Control of Aero engine Distributed Control System with Packet Dropout Compensator. *Procedia Eng.* **2011**, *15*, 618–623. [[CrossRef](#)]
- Kolmanovsky, I.V.; Jaw, L.C.; Merrill, W.; Van, H.T. Robust control and limit protection in aircraft gas turbine engines. In Proceedings of the 2012 IEEE International Conference on Control Applications (CCA), Dubrovnik, Croatia, 3–5 October 2012; pp. 812–819, ISBN 978-1-4673-4503-3. [[CrossRef](#)]
- Kratz, J.; Yedavalli, R.K. A Riccati equation based robust control design with application to a gas turbine engine leading toward distributed control. In Proceedings of the 50th AIAA/ASME/SAE/ASEE Joint Propulsion Conference, Cleveland, OH, USA, 28–30 July 2014; p. 3639. [[CrossRef](#)]
- Najimi, E.; Ramezani, M.H. Robust control of speed and temperature in a power plant gas turbine. *ISA Trans.* **2012**, *51*, 304–308. [[CrossRef](#)] [[PubMed](#)]
- Turso, J.; Litt, J. Intelligent, Robust Control of Deteriorated Turbofan Engines via Linear Parameter Varying Quadratic Lyapunov Function Design. In Proceedings of the AIAA 1st Intelligent Systems Technical Conference, Chicago, IL, USA, 20–22 September 2004; p. 6363. [[CrossRef](#)]
- Pan, M.; Zhang, K.; Chen, Y.H.; Huang, J. A New Robust Tracking Control Design for Turbofan Engines: H_∞/Leitmann Approach. *Appl. Sci.* **2017**, *7*, 439. [[CrossRef](#)]
- Marcos, A. Revisiting the aircraft C* control law: A comparison between classical and structured H-infinity designs. In Proceedings of the 2017 IEEE Conference on Control Technology and Applications (CCTA), Mauna Lani, HI, USA, 27–30 August 2017; pp. 2114–2119, ISBN 978-1-5090-2182-6. [[CrossRef](#)]
- Garcia, G.A.; Kashmiri, S.; Shukla, D. Nonlinear control based on H-infinity theory for autonomous aerial vehicle. In Proceedings of the 2017 International Conference on Unmanned Aircraft Systems (ICUAS), Miami, FL, USA, 13–16 June 2017; pp. 336–345, ISBN 978-1-5090-4495-5. [[CrossRef](#)]

17. You, S.S.; Lim, T.W.; Kim, J.Y.; Choi, H.S. Robust control synthesis for dynamic vessel positioning. *Proc. Inst. Mech. Eng. Part M J. Eng. Marit. Environ.* **2017**, *231*, 98–108. [[CrossRef](#)]
18. Bayas, A.; Škrjanc, I.; Sáez, D. Design of fuzzy robust control strategies for a distributed solar collector field. *Appl. Soft Comput.* **2018**, *71*, 1009–1019. [[CrossRef](#)]
19. Wang, X.; Yaz, E.E.; Schneider, S.C.; Yaz, Y.I. H_2 – H_∞ control of discrete-time nonlinear systems using the state-dependent Riccati equation approach. *Syst. Sci. Control Eng.* **2017**, *5*, 215–223. [[CrossRef](#)]
20. Andoga, R.; Főző, L.; Judičák, J.; Bréda, R.; Szabo, S.; Rozenberg, R.; Džunda, M. Intelligent Situational Control of Small Turbojet Engines. *Int. J. Aerosp. Eng.* **2018**, *2018*, 8328792. [[CrossRef](#)]
21. Főző, L.; Andoga, R.; Beneda, K.; Kolesár, J. Effect of operating point selection on non-linear experimental identification of iSTC–21v and TKT–1 small turbojet engines. *Period. Polytech. Transp. Eng.* **2017**, *45*, 141–147. [[CrossRef](#)]
22. Komjátý, M.; Főző, L.; Andoga, R. Experimental identification of a small turbojet engine with variable exhaust nozzle. In Proceedings of the 2015 16th IEEE International Symposium on Computational Intelligence and Informatics (CINTI), Budapest, Hungary, 19–21 November 2015; pp. 65–69, ISBN 978-1-4673-8519-0.
23. Madarász, L.; Andoga, R.; Češkovič, M.; Laššák, M.; Šmelko, M.; Főző, L. Advanced Approaches in Modeling of Complex Electromechanical Systems. In Proceedings of the CINTI 2011: 12th IEEE International Symposium on Computational Intelligence and Informatics, Budapest, Hungary, 21–22 November 2011; pp. 541–544, ISBN 978-1-4577-0043-9.
24. Nyulászi, L.; Madarász, L. Experimental Identification of the Small Turbojet Engine MPM-20. In Proceedings of the CINTI 2014: 15th IEEE International Symposium on Computational Intelligence and Informatics, Budapest, Hungary, 19–21 November 2014; pp. 497–501, ISBN 978-1-4799-5338-7.
25. Mackenroth, U. *Robust Control Systems: Theory and Case Studies*; Springer: Berlin/Heidelberg, Germany, 2013; ISBN 978-3-662-09775-5.
26. Glover, K.; McFarlane, D. Robust stabilization of normalized coprime factor plant descriptions with H /sub infinity/-bounded uncertainty. *IEEE Trans. Autom. Control* **1989**, *34*, 821–830. [[CrossRef](#)]
27. Precup, R.-E.; David, R.-C.; Petriu, E.M. Grey wolf optimizer algorithm-based tuning of fuzzy control systems with reduced parametric sensitivity. *IEEE Trans. Ind. Electron.* **2017**, *64*, 527–534. [[CrossRef](#)]
28. Várkonyi, T.A.; Tar, J.; Rudas, I. Improved stabilization for robust fixed point transformations-based controllers. *J. Adv. Comput. Intell. Intell. Inform.* **2013**, *17*, 418–424. [[CrossRef](#)]
29. Lacerda, M.J.; Tognetti, E.S.; Oliveira, R.C.; Peres, P.L. A new approach to handle additive and multiplicative uncertainties in the measurement for LPV filtering. *Int. J. Syst. Sci.* **2016**, *47*, 1042–1053. [[CrossRef](#)]



© 2019 by the authors. Licensee MDPI, Basel, Switzerland. This article is an open access article distributed under the terms and conditions of the Creative Commons Attribution (CC BY) license (<http://creativecommons.org/licenses/by/4.0/>).